Ferroelectric liquid-crystal and solid phases formed by strongly interacting dipolar soft spheres

Dongqing Wei and G. N. Patey
Department of Chemistry, University of British Columbia, Vancouver, British Columbia, Canada V6T 1Z1
(Received 29 April 1992)

Molecular-dynamics simulation results are reported for systems of strongly interacting dipolar soft spheres. Calculations have been carried out along two isotherms and the structure of the liquid-crystal and solid phases obtained is described in detail. It is found that in addition to the ferroelectric nematic phase we previously reported [Phys. Rev. Lett. **68**, 2043 (1992)], liquid crystals with columnar order can also be obtained. The model freezes to form a ferroelectric solid which is shown to have a tetragonal I crystal structure. The influence of different boundary conditions upon the simulation results is also discussed.

PACS number(s): 64.70.Md, 77.80.−e, 82.20.Wt

I. INTRODUCTION

In a recent Letter [1] we reported molecular-dynamics (MD) calculations which demonstrated that a simple dipolar soft-sphere fluid can form an orientationally ordered liquid-crystal phase if the dipolar interactions are sufficiently strong. These simulations established that dipolar forces alone are sufficient to create an orientationally ordered fluid confirming a suggestion first made by Born [2] and answering a question which has persisted for many years in liquid-crystal literature [3]. Furthermore, it was shown that at the temperature and densities considered the liquid-crystal phase was a ferroelectric nematic [4] liquid crystal showing no evidence of any long-range spatial order. This was a demonstration that a ferroelectric nematic liquid crystal could exist as a true liquid-crystal phase for a completely Hamiltonian model. This observation provided strong support for recent suggestions [5–7] that it might be possible to construct ferroelectric nematic liquid crystals in the laboratory.

The purpose of the present paper is to give more detailed results for the dipolar soft-sphere model. We have carried out extensive molecular-dynamics calculations along different isotherms; here we describe the phase behavior and the structure of the liquid-crystal and solid states. Liquid crystals with columnar order are found at temperatures lower than that considered in [1]. The influence of different boundary conditions upon the simulation results is also investigated and discussed.

The remainder of this paper is divided into three parts. The model and simulation method are briefly described in Sec. II, the results are given in Sec. III, and our conclusions are summarized in Sec. IV.

II. MODEL AND SIMULATION METHOD

The model we consider consists of soft spheres with point dipoles embedded at the center. The pair potential for this model can be expressed in the form

$$u(12) = u_{\rm ss}(r) + u_{\rm DD}(12) \ , \tag{2.1a}$$

where

$$u_{\rm ss}(r) = 4\varepsilon_{\rm ss}(\sigma/r)^{12} \tag{2.1b}$$

is the soft-sphere potential and

$$u_{\rm DD}(12) = -3(\boldsymbol{\mu}_1\cdot\boldsymbol{r})(\boldsymbol{\mu}_2\cdot\boldsymbol{r})/r^5 + \boldsymbol{\mu}_1\cdot\boldsymbol{\mu}_2/r^3 \tag{2.1c}$$

is the dipole-dipole interaction. The parameters $\varepsilon_{\rm ss}$ and σ characterize the soft-sphere potential, $\boldsymbol{\mu}_i$ is the dipole moment of particle i, $\boldsymbol{r} = \boldsymbol{r}_2 - \boldsymbol{r}_1$, and r is the magnitude of $\boldsymbol{r}$. We emphasize that the only angle-dependent term in Eq. (2.1a) is the dipole-dipole interaction and hence orientational ordering can come only through the dipolar forces. We also remark that our choice of dipolar soft spheres rather than the more common Stockmayer model (i.e., dipolar Lennard-Jones particles) is not accidental. In the present study we are primarily interested in systems where the dipolar interactions are strong enough to produce orientationally ordered phases and for such systems the usual Stockmayer fluids tend not to be stable giving negative pressures at liquid densities.

Kusalik [8] has carried out extensive molecular-dynamics calculations for *isotropic* dipolar soft-sphere fluids and has given a very useful analysis of simulation details. We have used similar methods and for the same state parameters our results are in excellent quantitative agreement with those of Kusalik.

In all calculations we employed the periodic boundary conditions (PBC's) of de Leeuw, Perram, and Smith [9] and the long-range dipolar interactions were taken into account using the Ewald summation method. This amounts to replacing the dipole-dipole potential with the effective interaction [8, 9]

$$u_{\rm DD}^{\rm PBC}(12;\epsilon') = -(\boldsymbol{\mu}_1\cdot\boldsymbol{\nabla})(\boldsymbol{\mu}_2\cdot\boldsymbol{\nabla})\Psi(\boldsymbol{r}) + \frac{4\pi}{(2\epsilon'+1)L^3}\boldsymbol{\mu}_1\cdot\boldsymbol{\mu}_2 \ , \tag{2.2a}$$

where

$$\Psi(\boldsymbol{r}) = \frac{1}{L}\sum_{\boldsymbol{n}} \frac{\operatorname{erfc}(\alpha|\boldsymbol{r}/L+\boldsymbol{n}|)}{|\boldsymbol{r}/L+\boldsymbol{n}|} + \frac{1}{\pi L}\sum_{\boldsymbol{n}\ (\neq \boldsymbol{0})} \frac{1}{n^2}\exp\left(\frac{-\pi^2 n^2}{\alpha^2} + \frac{2\pi i}{L}\boldsymbol{n}\cdot\boldsymbol{r}\right) , \tag{2.2b}$$

ϵ' is the dielectric constant of the surrounding continuum [9], L is the length of the cubic simulation cell, erfc is the error-function complement, α is a parameter adjusted to facilitate convergence, and the sum on $\boldsymbol{n}$ is over lattice vectors. The calculation of $\Psi(\boldsymbol{r})$ depends upon the truncation of the real and Fourier space sums [i.e., the first and second terms in Eq. (2.2b), respectively] and the value of the convergence parameter α. Further, the short-range soft-sphere interactions can be truncated at some cutoff radius R_c. Kusalik has investigated the convergence of the Ewald sum for different parameter sets with different numbers of particles and we have followed his suggestions. In the present calculations, we used $R_c = L/2$, $\alpha = 6.4$, retained only the $\boldsymbol{n} = (0,0,0)$ term in the real space sum, and included terms up to $n^2 = 54$ in the Fourier space sum. Calculations with other parameter sets were also carried out to verify that our results were not sensitive to details of the particular set chosen.

The MD calculations were performed at constant temperature employing Gaussian isokinetic equations of motion [10] as described by Kusalik [8]. The orientational coordinates of the particles were expressed in terms of quaternion parameters and the equations of motion were integrated using a fourth-order Gear algorithm. The reduced time step $\Delta t^* = \Delta t/\sqrt{m\sigma^2/\varepsilon_{\rm ss}} = 0.0025$ (m is the mass of a particle) was employed in all calculations.

In order to distinguish fluid and solid phases, we calculated the mean-square displacement $\langle|\boldsymbol{r}_i(t) - \boldsymbol{r}_i(0)|^2\rangle$, where $\boldsymbol{r}_i(t)$ is the position vector of molecule i at time t. For fluids the mean-square displacement continually increases with time varying linearly at long times according to the Einstein relationship [11]

$$\langle|\boldsymbol{r}_i(t) - \boldsymbol{r}_i(0)|^2\rangle = 6Dt , \tag{2.3}$$

where D is the diffusion coefficient. We note that in an orientationally ordered liquid-crystal phase the diffusion may not be isotropic and D is then given by $(D_{\parallel} + 2D_{\perp})/3$, where $D_{\parallel}$ and $D_{\perp}$ are the diffusion constants parallel and perpendicular to the director. For solids, the mean-square displacement becomes constant rather than continually increasing with time.

The possible existence of orientationally ordered phases was monitored by calculating the usual equilibrium first- and second-rank orientational order parameters, $\langle P_1\rangle$ and $\langle P_2\rangle$, respectively. Of course, for isotropic fluids both order parameters are zero. For ordinary nonferroelectric nematics $\langle P_2\rangle \neq 0$, $\langle P_1\rangle = 0$. For ferroelectric nematics both $\langle P_2\rangle$ and $\langle P_1\rangle$ must be nonzero. The instantaneous second-rank order parameter P_2 was taken to be the largest eigenvalue of the ordering matrix $\mathbf{Q}$ with elements given by [11]

$$Q_{\alpha\beta} = \frac{1}{N}\sum_{i=1}^{N} \tfrac{1}{2}(3\mu_\alpha^i\mu_\beta^i - \delta_{\alpha\beta}) , \tag{2.4}$$

where N is the number of particles in the simulation cell and μ_α^i is the α component of the unit vector $\hat{\boldsymbol{\mu}}_i$. The corresponding eigenvector is the instantaneous director $\hat{\boldsymbol{d}}$ and the instantaneous first-rank order parameter P_1 is defined by [7, 12]

$$P_1 = \frac{1}{N}\left|\sum_{i=1}^{N} \hat{\boldsymbol{\mu}}_i \cdot \hat{\boldsymbol{d}}\right| . \tag{2.5}$$

The equilibrium order parameters are the ensemble averages of P_1 and P_2.

For axially symmetric dipolar particles, the angle-dependent pair distribution function $g(12)$ can be expanded in the form

$$g(12) = \sum_{m,n,l} g^{mnl}(r)\Phi^{mnl}(12) , \tag{2.6}$$

where the $\Phi^{mnl}(12)$ are rotational invariants defined as in earlier work [13]. The projection $g^{000}(r)$ is the usual radial distribution function and tends to 1 as $r \to \infty$ in both isotropic and nematic phases. In orientationally disordered isotropic fluids all other $g^{mnl}(r)$ projections will decay to zero as $r \to \infty$. However, for a nematic phase it is not difficult to show that projections of the form $g^{mm0}(r)$ must obey the asymptotic relationship

$$g^{mm0}(r) \sim (2m+1)\langle P_m\rangle^2 , \ r \to \infty , \tag{2.7}$$

where $\langle P_m\rangle$ is the mth-rank order parameter. Thus, for nonferroelectric nematic phases $g^{mm0}(r)$ will approach a constant at large r for even m but decay if m is odd. For ferroelectric systems the projections will approach constants for both even and odd values of m. In the present simulations we have calculated $g^{000}(r)$, $g^{110}(r)$, $g^{112}(r)$, and $g^{220}(r)$ providing both structural information and an alternative route to the order parameters for nematic liquid crystals.

In order to better establish the structure of orientationally ordered phases, we have calculated the longitudinal and transverse pair correlation functions, $g_{\parallel}(r_{\parallel})$ and $g_{\perp}(r_{\perp})$, respectively. Here $r_{\parallel}$ and $r_{\perp}$ are components of the interparticle vector $\boldsymbol{r}$ parallel and perpendicular to the director. These functions measure positional correlations in directions parallel and perpendicular to the director and are very sensitive to any long-range spatial correlations. From the properties of these correlation functions one can readily determine if the liquid crystal is a simple nematic one or if it has columnar or smectic order [14, 15]. Very briefly, for a nematic phase both distribution functions will have at most weak short-range structure. In a columnar phase there is no translational order parallel to the director and hence $g_{\parallel}(r_{\parallel})$ will have relatively weak liquidlike features. On the other hand, $g_{\perp}(r_{\perp})$ can be expected to show solidlike structure resulting from two-dimensional order in planes perpendicular to the columns. The layered structure of a smectic phase leads to periodic oscillations in $g_{\parallel}(r_{\parallel})$ while $g_{\perp}(r_{\perp})$ re-

mains liquidlike. In solids both functions will have long-range order and for the present model we find that they give a very useful indication of the crystal structure.

III. RESULTS

Dipolar soft-sphere fluids can be characterized by specifying the reduced density $\rho^* = \rho\sigma^3$, the reduced temperature $T^* = kT/\varepsilon_{ss}$, and the reduced dipole moment $\mu^* = (\mu^2/\varepsilon_{ss}\sigma^3)^{1/2}$, where $\rho = N/V$, V is the volume, T is the absolute temperature, and k is the Boltzmann constant. In all calculations we have used the reduced dipole moment $\mu^* = 3$ which, if $\sigma = 3.0$ Å and $T = 298$ K, corresponds to a molecular dipole moment of approximately 2.7 D.

Most simulations were performed with 256 particles but some 108 and 864 particle calculations were done to investigate any dependence upon the number of particles. Typically, runs were begun with randomly oriented particles on a face centered cubic lattice and were equilibrated for about 40 000 time steps. However, some calculations particularly at lower temperatures and/or near phase transitions were run for much longer times (up to 200 000 timesteps) in order to ensure that the equilibrium state was reached. Averages were then collected for at least another 100 000 time steps. The standard deviations were estimated by dividing the final 100 000 time steps up into ten equal blocks and assuming for statistical purposes that the block averages constitute independent measurements of the physical properties of interest.

For the present model, the dielectric constants of the dense isotropic liquids are large and increase very rapidly in the vicinity of the isotropic to ferroelectric liquid-crystal transition (see Fig. 4 below). Therefore, we would expect the usual Ewald-Kornfeld boundary conditions which correspond to $\epsilon' = \infty$ to give a good approximation to infinite-system behavior as the transition is approached. As noted in [1] and below, if ϵ' is large, the exact value employed in the simulations is not critical. In order to determine the maximum effect of varying ϵ' we have also carried out some calculations with $\epsilon' = 1$. It is most convenient to discuss both cases separately.

A. Simulations with $\epsilon' = \infty$

Here we discuss the phase behavior and structure along two isotherms $T^* = 1.35$ and $T^* = 1.0$. All results given in this section were obtained with $\epsilon' = \infty$. At $T^* = 1.35$, some simulations were carried out with $\epsilon' = 225$ and the results obtained did not differ significantly from those found with $\epsilon' = \infty$.

It is convenient to begin our discussion with the $T^* = 1.35$ results. The order parameters, reduced pressures, $\langle P\rangle\sigma^3/\varepsilon_{ss}$, and reduced potential energies $\langle U\rangle/N\varepsilon_{ss}$ obtained at this temperature are shown in Figs. 1(a), 2(a), and 3(a), respectively. At $T^* = 1.35$ all three functions indicate the presence of two phase transitions. From Fig. 1(a) we see that both the first- and second-rank order parameters increase rather sharply at two densities ($\rho^* \approx 0.65$ and 0.87) and by considering the behavior

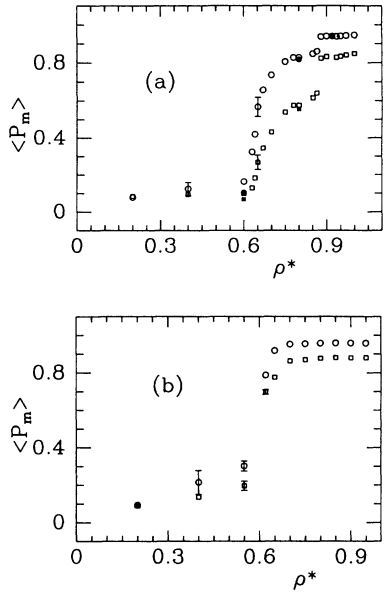

FIG. 1. The orientational order parameters as a function of the density for (a) $T^* = 1.35$ and (b) $T^* = 1.0$. The open circles and squares are $\langle P_1\rangle$ and $\langle P_2\rangle$, respectively, obtained with 256 particles. The solid circles and squares in (a) are $\langle P_1\rangle$ and $\langle P_2\rangle$, respectively, obtained with 864 particles. The error bars represent one estimated standard deviation and are about the size of the symbols in the ordered phases.

of the mean-square displacements [1] (typical results are shown in [1] and in Fig. 8, below) we conclude that the first phase transition is from an isotropic to a ferroelectric liquid and the second is a ferroelectric liquid to ferroelectric solid transition. In the pressure plot [Fig. 2(a)] the solid and liquid branches are very clear since the solidification is strongly first order and the pressure change is obvious at the freezing transition. The change in pressure at the isotropic-to-liquid-crystal transition is much smaller but with care and accurate calculations it is possible (see expanded scale) to distinguish isotropic and liquid-crystal branches. The average potential energies shown in Fig. 3(a) are also not monotonic in density and the transitions are accompanied by energy decreases.

For the Ewald-Kornfeld boundary conditions employed in the present calculations, the appropriate formula for the dielectric constant ϵ of an *isotropic* fluid is [9, 16]

$$\epsilon - 1 = \frac{4\pi}{3VkT}(\langle \boldsymbol{M}^2\rangle - \langle \boldsymbol{M}\rangle^2) , \tag{3.1}$$

where $\boldsymbol{M}$ is the total dipole moment of the simulation cell. In principle, in order to obtain reliable estimates of the dielectric constants the simulations should be long enough to yield $\langle \boldsymbol{M}\rangle^2/\langle \boldsymbol{M}^2\rangle \approx 0$. In practice, this is difficult particularly for the fluids of strongly interacting particles we consider. Nevertheless, at $T^* = 1.35$ we have carried out several calculations of sufficient length (i.e., 300 000 time steps) to ensure that $\langle \boldsymbol{M}\rangle^2/\langle \boldsymbol{M}^2\rangle \approx 0.1$. The results obtained for ϵ are shown in Fig. 4. We see that as expected the dielectric constant increases very rapidly as the ferroelectric transition is approached.

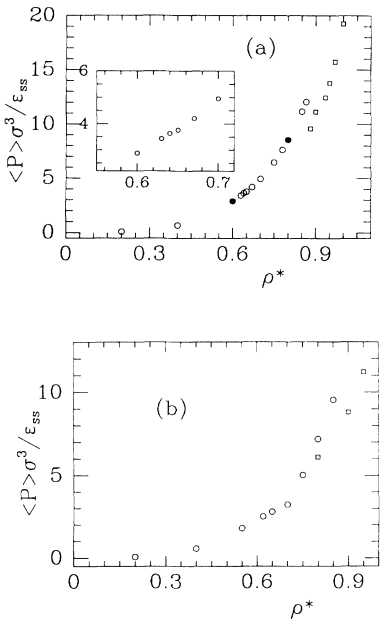

FIG. 2. The reduced pressure as a function of the density for (a) $T^* = 1.35$ and (b) $T^* = 1.0$. The open and solid circles [in (a) only] represent liquid-state results obtained with 256 and 864 particles, respectively. The solid-state results are shown as open squares. The estimated standard deviations are much smaller than the symbols.

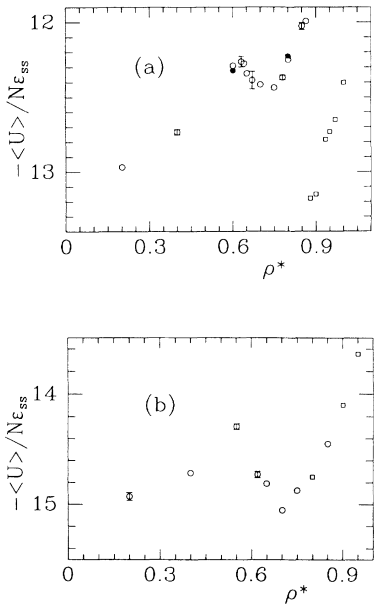

FIG. 3. The reduced potential energy as a function of the density for (a) $T^* = 1.35$ and (b) $T^* = 1.0$. The symbols are as in Fig. 2. The error bars represent one estimated standard deviation and are about the size of the symbols in the ordered phases.

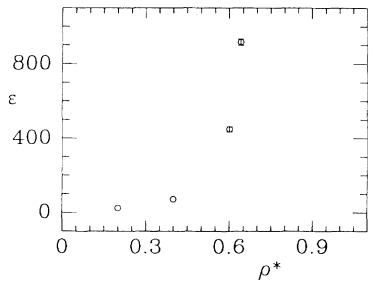

FIG. 4. The dielectric constant as a function of the density for $T^* = 1.35$. The error bars represent one estimated standard deviation.

The pair distribution function projections $g^{000}(r)$, $g^{110}(r)$, $g^{112}(r)$, and $g^{220}(r)$ [cf. Eq. (2.6)] obtained at $T^* = 1.35$ are shown in Fig. 5. Curves for isotropic, liquid crystal, and solid phases are included. The projection $g^{000}(r)$ is the usual radial distribution function, and it is also useful to note that $g^{112}(r)$ is proportional to the average interaction energy between a pair of dipoles at separation r [13].

From Fig. 5 we see that both $g^{110}(r)$ and $g^{220}(r)$ decay to zero as expected in the isotropic fluid and approach constants at large r in the liquid crystal phase. Using Eq. (2.7), it is easy to verify that the constants obtained are consistent with the values of $\langle P_1 \rangle$ and $\langle P_2 \rangle$ calculated directly. Furthermore, we see that all four projections show no evidence of long-range spatial order in the liquid-crystal phase. These observations also hold for calculations with 864 particles [1] and strongly suggest that at $T^* = 1.35$ the liquid-crystal phase is a ferroelectric nematic. This is confirmed by the distribution functions parallel and perpendicular to the director, $g_{\parallel}(r_{\parallel})$ and $g_{\perp}(r_{\perp})$, respectively, shown in Fig. 6. For the liquid-crystal phase these functions are completely without structure and are not distinguishable from the isotropic case. This indicates that the liquid-crystal phase is simply nematic and does not have the long-range spatial order associated with smectic or columnar phases [14, 15]. We shall see below that a liquid crystal with columnar order does exist at lower temperatures.

From Fig. 6, we see that in the solid both $g_{\parallel}(r_{\parallel})$ and $g_{\perp}(r_{\perp})$ exhibit long-range order. Both functions are oscillatory and the period is $\sim 0.5\sigma$ for $g_{\parallel}(r_{\parallel})$ and $\sim 1\sigma$ for $g_{\perp}(r_{\perp})$. The structural features of $g_{\parallel}(r_{\parallel})$ and $g_{\perp}(r_{\perp})$ as well as those of the $g^{mnl}(r)$ are completely consistent with a ferroelectric tetragonal I crystal [17] defined by the unit cell shown in Fig. 7. The cell dimensions 1.0σ and 1.5σ as shown in the figure give an essentially exact fit to the structural features. The projection $g^{112}(r)$ (Fig. 5) is particularly useful since it shows where the average pair interactions are attractive or repulsive and it is easy to identify the lattice separations giving rise to the different structural features. For example, the first peak obviously comes from the attractive interactions between aligned near neigbors at 1.0σ, and the first mimimum at $\sim 1.17\sigma$ comes from the repulsive interactions between particles on the corners and those at the body center of the unit cell. All other maxima and minima in $g^{112}(r)$

can be explained by considering the interaction between particles at different lattice points.

With the solid structure in mind, it is useful to consider again briefly the nature of the liquid crystal. From Fig. 5 we see that at short range the projections of the pair distribution obtained in the nematic phase qualitatively resemble those of the solid. Specifically, one notes that the first peak in $g^{000}(r)$, $g^{110}(r)$, and $g^{220}(r)$ tends to be rounded rather than sharp as in the isotropic phase. Furthermore, the structure of $g^{112}(r)$ indicates average repulsive interactions at $r \approx 1.17\sigma$ which also occurs in the solid but not in the isotropic system. These observations indicate that there are short-range spatial correlations in the ferroelectric nematic which are similar to the arrangements found in the tetragonal I crystal.

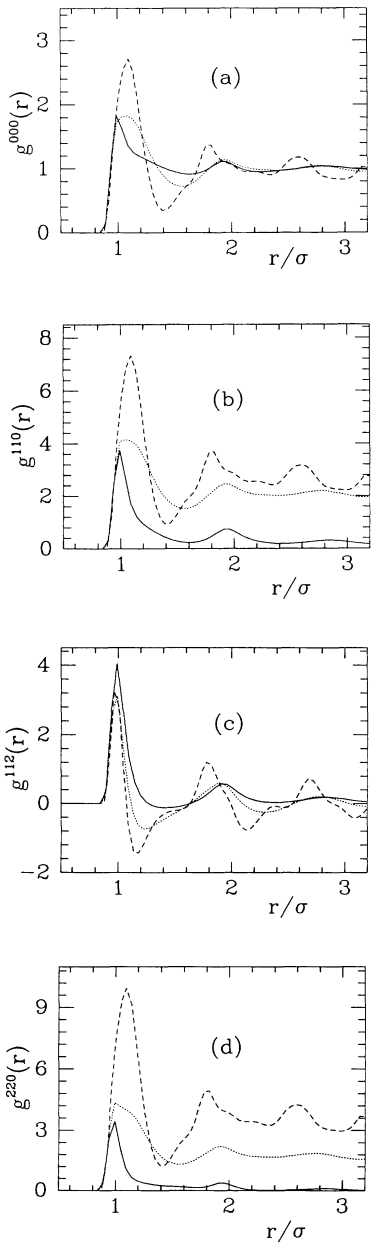

FIG. 5. Projections of the pair distribution functions at $T^* = 1.35$. All results were obtained with 256 particles and the solid, dotted, and dashed curves are for $\rho^* = 0.6$ (isotropic), 0.8 (nematic), and 1.0 (solid), respectively.

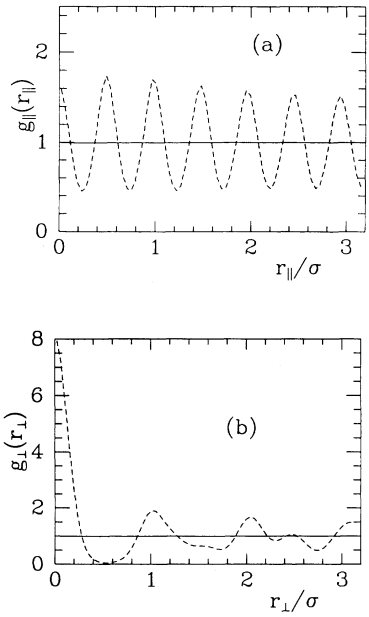

FIG. 6. The pair distribution functions parallel and perpendicular to the director at $T^* = 1.35$. The curves are as in Fig. 5. The results in the isotropic ($\rho^* = 0.6$) and nematic ($\rho^* = 0.8$) contain no structure and result in the flat line at 1.

The results obtained at $T^* = 1$ are shown in Figs. 1(b), 2(b), 3(b), 8, 9, and 10. At this temperature the MD calculations proved more difficult to converge than at $T^* = 1.35$ and even with very long runs it was difficult to determine very precisely the densities at which phase transitions occur. This was particularly true of the liquid crystal to solid transition which occurs somewhere in the vicinity of $\rho^* \approx 0.8$. It can be seen from the pressure plot [Fig. 2(b)] that the liquid and solid branches have a considerable region of overlap where different simulations at the same density can result in either liquid-crystal or solid phases depending to some extent upon the starting configuration. For example, starting from a lattice or from another run at a higher temperature may give different results in this region. Nevertheless, with persistence, and making use of all information contained in the figures a good qualitative picture of the phase behavior can be deduced.

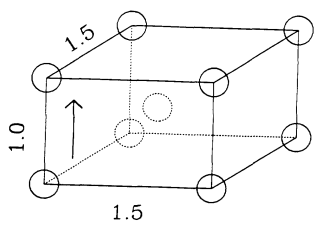

FIG. 7. The tetragonal I unit cell. The numbers give the cell dimensions in units of σ and the arrow indicates the direction of the dipoles.

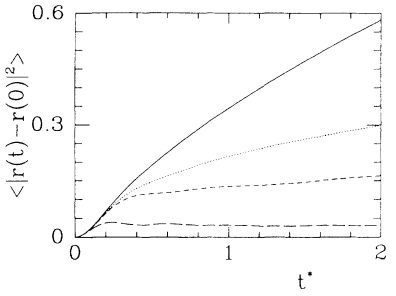

FIG. 8. The mean-square displacement as a function of t^* for different phases at $T^* = 1.0$. The solid, dotted, dashed, and broken lines are for $\rho^* = 0.55$ (isotropic), 0.65 (nematic), 0.70 (columnar), and 0.95 (solid), respectively.

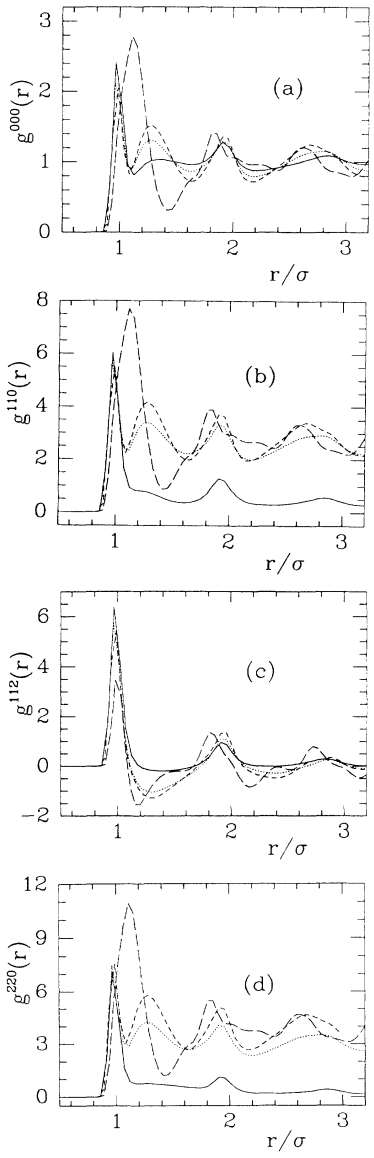

FIG. 9. Projections of the pair distribution functions at $T^* = 1.0$. All results were obtained with 256 particles. The solid, dotted, dashed, and broken lines are for $\rho^* = 0.55$ (isotropic), 0.65 (nematic), 0.70 (columnar), and 0.95 (solid), respectively.

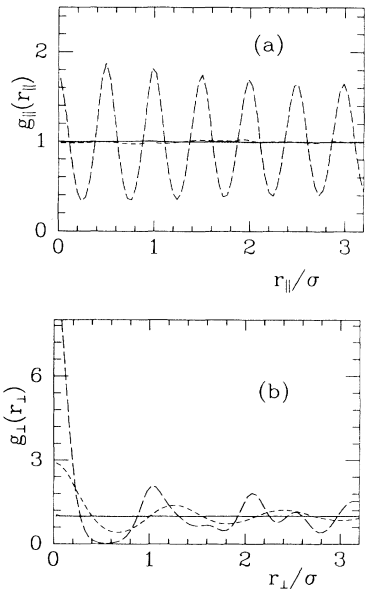

FIG. 10. The pair distribution functions parallel and perpendicular to the director at $T^* = 1.0$. The solid, dotted, dashed, and broken lines are for $\rho^* = 0.55$ (isotropic), 0.65 (nematic), 0.70 (columnar), and 0.95 (solid), respectively.

The mean-square displacements (Fig. 8) indicate that at densities less than $\rho^* \approx 0.8$ the system exists only as fluid states. From the order parameters plotted in Fig. 1(b) it is evident that an isotropic to ferroelectric liquid-crystal transition occurs at $\rho^* \approx 0.6$. For densities between $\rho^* \approx 0.6$ and 0.68, the $g_{\parallel}(r_{\parallel})$ and $g_{\perp}(r_{\perp})$ (Fig. 10) exhibit no structure whatsoever indicating that in this density range the liquid crystal phase is a ferroelectric nematic with no spatial order. For liquid crystals at densities higher than $\rho^* \approx 0.7$, $g_{\parallel}(r_{\parallel})$ remains essentially structureless but $g_{\perp}(r_{\perp})$ exhibits an oscillatory behavior. These features are characteristic of columnar order [14]. The existence of columnar order for the dipolar model is not surprising because we would expect the dipoles to have a tendency to form energetically favoured columns at low temperatures.

The projections plotted in Fig. 9 indicate that the short-range structure of the nematic phase differs from the $T^* = 1.35$ case. From Fig. 9 we see that the first maximum in $g^{000}(r)$, $g^{110}(r)$, and $g^{220}(r)$ is now split into a very sharp peak at $r \approx 1\sigma$ and a much broader peak at $r \approx 1.3\sigma$. The sharpness of the first peak strongly suggests that some level of "dimerization" not present at $T^* = 1.35$ occurs at $T^* = 1$. This is consistent with the formation of columnar order at higher densities as discussed above. The broad peak at $r \approx 1.3\sigma$ which occurs weakly in the isotropic system and strongly in the liquid crystals must reflect "dimer-dimer" or "column-column" (at the higher densities) correlations. In the solid phase the initial peaks collapse into a single maximum and all structural features are similar to those observed in the solid at $T^* = 1.35$, $\rho^* = 1.0$. This is also true of $g_{\parallel}(r_{\parallel})$ and $g_{\perp}(r_{\perp})$, and the solid can be identified as a ferroelectric tetragonal I crystal as described above. In fact,

at $T^* = 1$, $\rho^* = 0.95$, the cell dimensions 1.0σ and 1.5σ again give a good fit to the structural properties.

Several other features of the results at $T^* = 1$ should be mentioned. From Fig. 1(b) we note that, unlike the $T^* = 1.35$ case [Fig. 1(a)], at the lower temperature the liquid crystal to solid transition is not marked by a significant jump in the order parameters. Further, from Fig. 3(b) we see that the freezing transition (at $\rho^* \approx 0.8$) is not accompanied by a sharp drop in the average energy as is observed for $T^* = 1.35$ [Fig. 3(a)]. These differences can be explained by the fact that the columnar liquids found for $\rho^* \geq 0.7$ are already highly ordered and hence the order parameters and energy do not differ much from those of the solid at the same density. Finally, we note that on the scale used in Fig. 2(b), the average pressure appears to turn up rather abruptly at the onset of columnar order (i.e., $\rho^* \approx 0.7$). However, at this temperature we have not attempted to identify branches associated with different fluid phases. Presumably, for the isotropic-nematic transition more detailed results would behave much as those obtained at $T^* = 1.35$ [Fig. 2(a)].

B. Simulations with $\epsilon' = 1$

In order to demonstrate the maximum effect of changing the parameter ϵ' in the effective PBC interaction given by Eq. (2.2a), we have carried out some simulations with $\epsilon' = 1$. This amounts to surrounding the "infinitely" periodic sample with a vacuum [9] and is extreme since, as shown above, for the present model the dielectric constants are very large in the dense fluid regime. Before discussing the results obtained, it is useful to consider the second term in Eq. (2.2a). This term obviously vanishes when $\epsilon' = \infty$ and makes its maximum contribution when $\epsilon' = 1$. Furthermore, it does not decay with separation and it is clear from the $\boldsymbol{\mu}_1 \cdot \boldsymbol{\mu}_2$ dependence that this term will favor antiparallel rather than parallel dipolar orientations. Thus, at the very least, we might anticipate a significant effect upon the ferroelectric behavior of the nematic phase when ϵ' is varied from ∞ to 1.

Calculations with 256 particles and $\epsilon' = 1$ did not give a clearly defined liquid-crystal phase at $T^* = 1.35$. However, a liquid crystal was obtained at $T^* = 1.1$ and therefore this is the isotherm which we will discuss in detail here. At this temperature simulations were carried out with 108, 256, and 864 particles and the results are shown in Figs. 11–15.

The order parameters, reduced pressures, and reduced potential energies obtained are plotted in Fig. 11. From the second-rank order parameter, we see that an isotropic-to-liquid-crystal transition occurs at $\rho^* \approx 0.67$, and the behavior of the reduced pressure indicates that solidification occurs somewhere in the vicinity of $\rho^* \approx 0.88$. However, the results differ from those obtained with large values of ϵ' in one very striking manner. Here the first-rank order parameter is within statistical error zero at all densities. Thus the liquid-crystal and solid phases are orientationally ordered but are not ferroelectric. As discussed above, this result is to some degree anticipated from the form of the effective pair potential with $\epsilon' = 1$. However, we shall see below that the liquid crystals obtained with $\epsilon' = 1$ and ∞ are not really as different as they appear to be at first. Although with $\epsilon' = 1$ the system is not globally ferroelectric, there are regions of local dipole order which grow as the system size is increased.

The projections of the pair distribution function found at different densities with 256 particles are given in Fig. 12. We see that at short range the projections qualitatively resemble the results found with $\epsilon' = \infty$ and $T^* = 1$ (Fig. 9). For example, the first maximum in $g^{000}(r)$, $g^{110}(r)$, and $g^{220}(r)$ is split into two peaks in the liquid crystal suggesting that at least some dimerization is occurring and, by examining $g_\perp(r_\perp)$ (Fig. 15), we see that there is also indication of columnar order.

Some insight into the structure of the liquid crystal found with $\epsilon' = 1$ can be obtained by examining Fig. 13 where we have plotted 108, 256, and 864 particle results for $g^{110}(r)$ and $g^{220}(r)$ at $\rho^* = 0.7$. For comparison results obtained at the same temperature and density with $\epsilon' = \infty$ and results for the isotropic liquid at $\rho^* = 0.6$ are also included. The projection $g^{110}(r)$ is very instructive. Although this function decays to zero in both the liquid-crystal and isotropic systems (consistent with the fact that $\langle P_1 \rangle = 0$ at all densities), it is obvious that the dipolar ordering in these phases is different. In the liq-

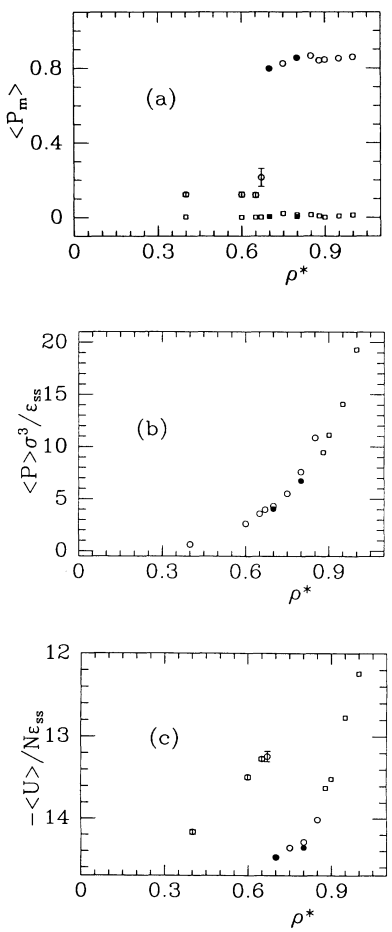

FIG. 11. The orientational order parameters, reduced pressure, and reduced potential energy obtained with $\epsilon' = 1$ and $T^* = 1.1$. The symbols are as in Figs. 1–3.

uid crystal $g^{110}(r)$ is large and positive at intermediate separations and decays to zero much more slowly than in the isotropic phase. This indicates a strong tendency towards local dipolar alignment. Furthermore, we see that $g^{110}(r)$ is significantly number dependent and that both the strength and range of the tendency towards dipolar alignment increases with the size of the sample. This behavior is consistent with the formation of ferroelectric domains in a sample which globally has no net dipole moment. Indeed, from the number dependence of the curves shown in Fig. 13 it is not unreasonable to conjecture that simulations with very large samples would yield

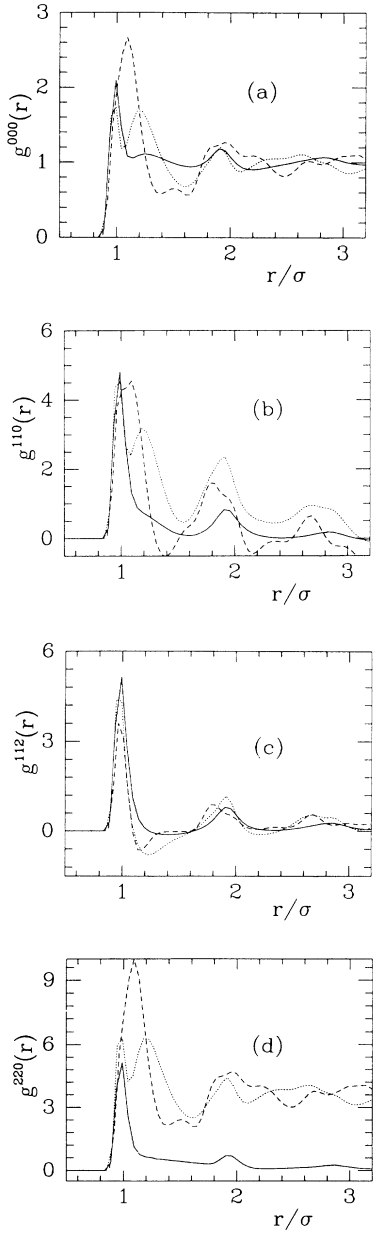

FIG. 12. Projections of the pair distribution functions obtained with $\epsilon' = 1$ and $T^* = 1.1$. All results were obtained with 256 particles and the solid, dotted, and dashed curves are for $\rho^* = 0.6$ (isotropic), 0.8 (columnar), and 1.0 (solid), respectively.

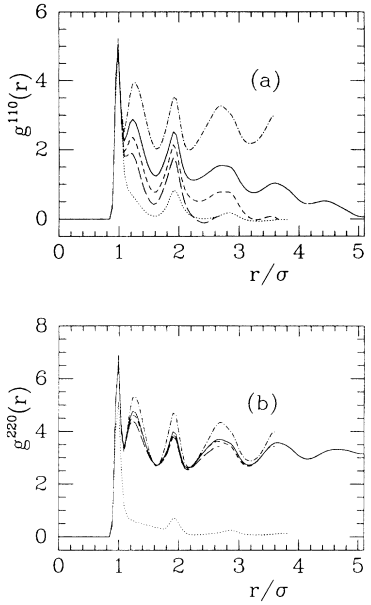

FIG. 13. A comparison between 108, 256, and 864 particle results for $g^{110}(r)$ and $g^{220}(r)$ in the liquid crystal obtained with $\epsilon' = 1$, $T^* = 1.1$, and $\rho^* = 0.7$. The solid, short-dash, and long-dash curves are 864, 256, and 108 particle results, respectively. The dash-dot curves are the results obtained at the same temperature and density with 256 particles and $\epsilon' = \infty$. The dotted curves are 256 particle results for the isotropic liquid at $\rho^* = 0.6$.

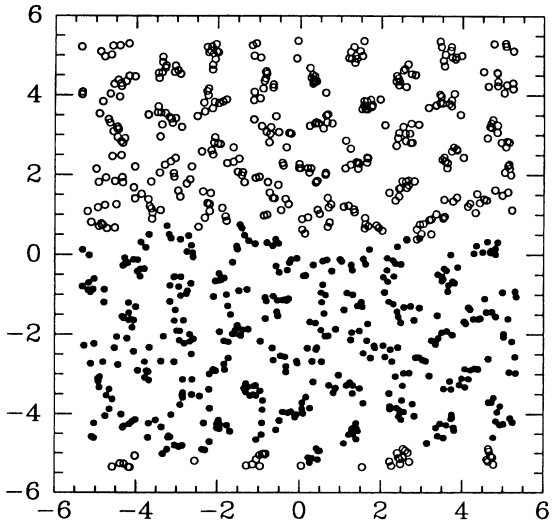

FIG. 14. A snapshot of the domain structure found in the liquid crystal with 864 particles, $\epsilon' = 1$, $T^* = 1.1$, and $\rho^* = 0.7$. The particles are projected onto a plane perpendicular to the director and the open and solid circles distinguish dipole which are "up" from those which are "down." The distances indicated on the axis are in units of σ and $L/2 = 5.36\sigma$. Also note, that under periodic boundary conditions the open circles at the bottom are actually part of the upper domain.

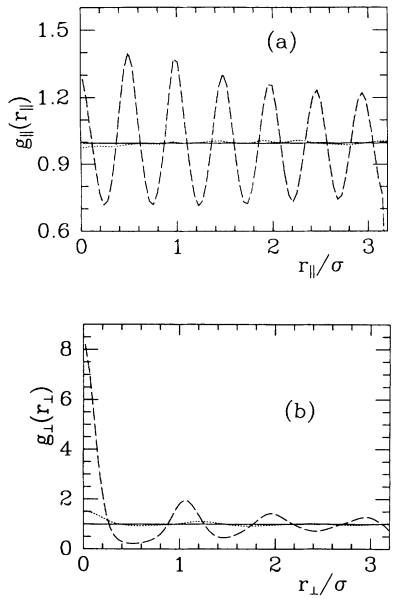

FIG. 15. The pair distribution functions parallel and perpendicular to the director obtained with $\epsilon' = 1$ and $T^* = 1.1$. The curves are as in Fig. 12.

results for $g^{110}(r)$ comparable with those obtained with $\epsilon' = \infty$ over a wide range of separations. In other words, for sufficiently large samples we would expect ferroelectric domains in which the local order is similar to that obtained with small samples and $\epsilon' = \infty$.

Further, from Fig. 13 we see that the $g^{220}(r)$ curve obtained with $\epsilon' = 1$ is qualitatively similar to the $\epsilon' = \infty$ result, although, as we might expect, the globally ferroelectric system is a little more ordered (note that for 256 particles $\langle P_2 \rangle = 0.84$ and 0.80 for $\epsilon' = \infty$ and 1, respectively). It is also evident that compared with $g^{110}(r)$ the number dependence of $g^{220}(r)$ is relatively weak. However, the results do move slowly in the direction of the $\epsilon' = \infty$ curve as the system size is increased. Again these observations are completely consistent with the formation of ferroelectric domains.

The domain structure can in fact be clearly seen by examining instantaneous configurations. In Fig. 14 we show a "snapshot" obtained by projecting all particles onto a plane perpendicular to the director but distinguishing dipoles which are "up" from those which are "down." In Fig. 14 this is done with open and solid circles and it is obvious from the pattern obtained that the system has split into two distinct domains and that the domain wall is sharp. The system illustrated in Fig. 14 contained 864 particles in the simulation cell but a similar picture emerges from calculations with 256 particles.

It is interesting to note that the existence of domain structure in ferroelectric crystals surrounded by vacuum is a well-known phenomenon [18] and that our results are entirely consistent with the solid-state picture. A rationalization based upon macroscopic energetic considerations is given in [18] and it is useful to briefly summarize the qualitative arguments here. One begins by considering a perfect (i.e., single domain) spherical ferroelectric crystal in vacuum. Charges induced on the external surface create a "depolarizing" electric field with energy proportional to the sample volume and to the square of the polarization. This field acts to destroy the uniform polarization of the perfect ferroelectric sample and the result is that the crystal becomes divided into domains having antiparallel directions of spontaneous polarization. Such states are favored over the perfect ferroelectric crystal because they reduce the energy of the depolarizing field. However, there is an energy increase associated with the formation of domain walls and hence domains will form only until the two effects are balanced.

This is clearly a very qualitative argument but it does give another perspective on our simulation results. The second term in the effective interaction given by Eq. (2.2a) can be regarded as a depolarizing field contribution. It has its maximum value when $\epsilon' = 1$ and the ferroelectric liquid crystals form antiparallel domains. It is also not difficult to understand why the particles in the simulation cell organize themselves into two equal domains with the domain wall running across the cell parallel to an axis orthogonal to the director as shown in Fig. 14. For a periodic system with a cubic central cell, this particular structural option completely destroys the polarization while creating only the minimum necessary interfacial area. For $\epsilon' = \infty$ (i.e., sample surrounded by a conductor) the depolarizing field is entirely "switched off" and single domain or perfect liquid crystals are obtained.

The functions $g_{\parallel}(r_{\parallel})$ and $g_{\perp}(r_{\perp})$ are given in Fig. 15. From the structure of these curves and of the projections shown in Fig. 12, the solid obtained with $\epsilon' = 1$ appears to be a somewhat distorted version of the tetragonal I crystal described above. However, in this case the crystal is not ferroelectric and snapshots of instantaneous configurations again revealed antiparallel ferroelectric domains similar to the situation in the liquid crystal. Evidence of the local ferroelectric order is also present in the structure of $g^{110}(r)$ and $g^{112}(r)$ which resemble the $\epsilon' = \infty$ results at short range.

IV. SUMMARY AND CONCLUSIONS

In this paper we have used molecular-dynamics simulations in order to explore the phase behavior of strongly interacting dipolar spheres. Periodic boundary conditions were employed and in most calculations the parameter ϵ' occurring in the effective PBC potential was taken to be infinity. This corresponds to the usual Ewald-Kornfeld boundary conditions and would seem to be the most appropriate choice for the present model which (at least in the isotropic phase) is characterized by very large dielectric constants. Furthermore, it was verified that if ϵ' is relatively large then the results obtained have little dependence upon the exact value used. Also, in order to determine the maximum effect of varying ϵ', some calculations were carried out using the lowest permissible value $\epsilon' = 1$.

With $\epsilon' = \infty$, calculations with 256 and 864 particles revealed no significant number dependence and simula-

tions were carried out along two isotherms, $T^* = 1.35$ and 1. As we previously reported [1], at $T^* = 1.35$ one obtains a ferroelectric nematic phase which freezes to form a ferroelectric solid as the density is increased. Here we have shown that this solid is a tetragonal I crystal with all dipoles aligned. The pair distribution function indicates that the short-range spatial correlations in the ferroelectric nematic phase resemble in some respects the structure of the tetragonal I crystal. We speculate that it is to some extent the development of these specific spatial correlations which stabilizes the ferroelectric nematic phase.

At $T^* = 1$, one also obtains a ferroelectric nematic phase. However, at this temperature there is evidence of particle "dimerization" and the liquid rapidly develops columnar order as the density is increased. Again, the system freezes into a ferroelectric tetragonal I crystal.

At first sight, the results obtained with $\epsilon' = 1$ appear to differ markedly from the $\epsilon' = \infty$ case. A liquid crystal characterized by large second-rank order parameters and some columnar structure was found at $T^* = 1.1$, but the system did not become ferroelectric and the first-rank order parameter was zero at all densities. However, the behavior of the system with $\epsilon' = 1$ does not differ as drastically from the $\epsilon' = \infty$ case as first appears. In the liquid crystal, the pair distribution function and snapshots of instantaneous configurations show the formation of two antiparallel ferroelectric domains which grow in size as the number of particles in the simulation cell is increased. Our results strongly suggest that for sufficiently large samples the local dipolar order within these domains would be very similar to that in the ferroelectric systems obtained with small samples and $\epsilon' = \infty$.

The solid formed with $\epsilon' = 1$ provides further support for this interpretation. Basically, a tetragonal I crystal is obtained, although now there are likely distortions since the dipoles are not all aligned. Again we find that groups of dipoles are locally aligned to form ferroelectric domains as in the liquid crystal. This is consistent with the macroscopic behavior of ferroelectric crystals in vacuum [18].

In summary, with PBC and $\epsilon' = \infty$ (or large) we find globally ferroelectric liquids and the physical properties of interest depend very little on sample size. With $\epsilon' = 1$, we obtain liquid crystals with no net polarization but with ferroelectric domains. We emphasize that both sets of calculations lead to essentially the same qualitative conclusions. In both cases strongly interacting dipolar soft spheres form orientationally ordered liquids and in both cases there is ferroelectric order. Whether or not the system is perfectly ferroelectric or is broken down into domains will depend upon how the long-range dipolar forces are treated or, in the present context, upon the value of ϵ'. However, we do not believe that this ϵ' dependence presents any serious questions for the physical interpretation of simulation results. The underlying reasons for the existence of domains in real ferroelectric materials are well understood and the same physical principles apply to the simulation studies.

ACKNOWLEDGMENTS

We thank Michel Gingras and Peter Kusalik for many helpful comments on an earlier draft of this paper. The financial support of the Natural Sciences and Engineering Research Council of Canada, and of the Network of Centres of Excellence Programme in association with the Natural Sciences and Engineering Research Council of Canada, is gratefully acknowledged.

[1] D. Wei and G.N. Patey, Phys. Rev. Lett. **68**, 2043 (1992).
[2] M. Born, Sitz. Phys. Math. **25**, 614 (1916); Ann. Phys. (Leipzig) **55**, 221 (1918).
[3] G.R. Luckhurst, in *The Molecular Physics of Liquid Crystals*, edited by G.R. Luckhurst and G.W. Gray (Academic, London, 1979), Chap. 4.
[4] For the present system, some may find the description "ferroelectric nematic phase" to be somewhat redundant since $\langle P_1 \rangle$ is the primary order parameter and, of course, if $\langle P_1 \rangle \neq 0$, $\langle P_2 \rangle$ cannot be zero. However, we include the word nematic not to imply the $\langle P_2 \rangle$ is the primary order parameter, but to indicate that the ferroelectric liquid crystal is a nematic phase in the sense that it has no long-range spatial order.
[5] L. Lei, Mol. Cryst. Liq. Cryst. **146**, 41 (1987); L.M. Leung and L. Lei, *ibid.* **146**, 71 (1987).
[6] P. Palffy-Muhoray, M.A. Lee, and R.G. Petshek, Phys. Rev. Lett. **60**, 2303 (1988).
[7] F. Biscarini, C. Zannoni, C. Chiccoli, and P. Pasini, Mol. Phys. **73**, 439 (1991).
[8] P.G. Kusalik, J. Chem. Phys. **93**, 3520 (1990).
[9] S.W. de Leeuw, J.W. Perram, and E.R. Smith, Annu. Rev. Phys. Chem. **37**, 245 (1986); Proc. R. Soc. London Ser. A **373**, 27 (1980); **A388** (1983).
[10] D.J. Evans and G.P. Morriss, Comp. Phys. Rep. **1**, 297 (1984); D.J. Evans, J. Chem. Phys. **78**, 3297 (1983); D.J. Evans, W.G. Hoover, B.H. Failor, B. Moran, and A.J.C. Ladd, Phys. Rev. A **28**, 1016 (1983).
[11] M.P. Allen and D.J. Tildesley, *Computer Simulation of Liquids* (Clarendon, Oxford, 1989), and references therein.
[12] If the present simple dipolar systems are ferroelectric, the polarization vector must be parallel to $\hat{\boldsymbol{d}}$. However, this need not be true in general.
[13] P.H. Fries and G.N. Patey, J. Chem. Phys. **82**, 429 (1985). The rotational invariants used here are defined by Eqs. (5) and (36) of this paper.
[14] A. Stroobants, H.N.W. Lekkerkerker, and D. Frenkel, Phys. Rev. A **36**, 2929 (1987).
[15] E. de Miguel, L.F. Rull, M.K. Chalam, and K.E. Gubbins, Mol. Phys. **74**, 405 (1991).
[16] M. Neumann, Mol. Phys. **50**, 841 (1983).
[17] P.W. Atkins, *Physical Chemistry*, 3rd ed. (Freeman, New York, 1986), p. 554.
[18] F. Jona and G. Shirane, *Ferroelectric Crystals* (Pergamon, New York, 1962), p. 45.